

Fano-Kondo effect in side-coupled double quantum dots at finite temperatures and the importance of the two-stage Kondo screening

Rok Žitko¹

¹*Jožef Stefan Institute, Jamova 39, SI-1000 Ljubljana, Slovenia*

(Dated: November 1, 2018)

We study the zero-bias conductance through the system of two quantum dots, one of which is embedded directly between the source and drain electrodes, while the second dot is side-coupled to the first one through a tunneling junction. Modeling the system using the two-impurity Anderson model, we compute the temperature-dependence of the conductance in various parameter regimes using the numerical renormalization group. We consider the non-interacting case, where we study the extent of the departure from the conventional Fano resonance line shape at finite temperatures, and the case where the embedded and/or the side-coupled quantum dot is interacting, where we study the consequences of the coexistence of the Kondo and Fano effects. If the side-coupled dot is very weakly interacting, the occupancy changes by two when the on-site energy crosses the Fermi level and a Fano-resonance-like shape is observed. If the interaction on the side-coupled dot is sizeable, the occupancy changes only by one and a very different line-shape results, which is strongly and characteristically temperature dependent. These results suggest an intriguing alternative interpretation of the recent experimental results study of the transport properties of the side-coupled double quantum dot [Sasaki et al., Phys. Rev. Lett. 103, 266806 (2009)]: the observed Fano-like conductance anti-resonance may, in fact, result from the two-stage Kondo effect in the regime where the experimental temperature is between the higher and the lower Kondo temperature.

PACS numbers: 72.15.Qm, 75.20.Hr, 73.23.-b, 73.40.Gk, 73.63.Kv

I. INTRODUCTION

In condensed-matter physics, the Fano resonance line shape^{1,2} is commonly observed in the low-temperature zero-bias conductance curves of various mesoscopic and nanoscale electronic devices when the energy of a weakly coupled discrete state is swept across the Fermi level using gate voltages. A prototype system where Fano physics may be observed consists of a single quantum dot side-coupled to a quantum wire^{3–15}. The Fano line shape results from an interference of the quantum amplitudes for the conduction pathway directly through the quantum wire without passing through the quantum dot and the indirect conduction pathway via the quantum dot. The first pathway plays the role of a broad background process, while the second corresponds to a resonant scattering channel. The conductance as a function of the discrete state energy level ϵ is well described by the Fano function

$$G(E) = a \frac{(E + q)^2}{1 + E^2} + b, \quad (1)$$

where

$$E = \frac{\epsilon - \epsilon_r}{\Gamma} \quad (2)$$

is a dimensionless energy that measures the energy difference from a resonance energy ϵ_r in units of the resonance half-width Γ , q is the Fano parameter given by the ratio of resonant and background scattering amplitudes, while a and b are some coefficients.⁷⁴ This energy dependence holds as long as the background conductance is constant over the width of the resonance; in experiments, curve fitting with Fano profile is typically done in an energy window of the order of several times Γ .

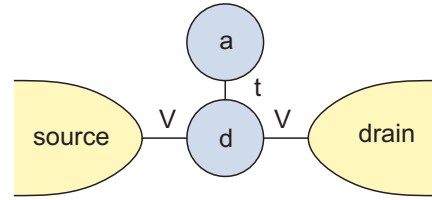


Figure 1: (Color online) Schematic representation of the double quantum dot nanostructure consisting of a quantum dot (d), embedded between the source and drain electrodes, and a side-coupled quantum dot (a).

The situation becomes more involved in a related structure consisting of two quantum dots, the first of which is embedded in the direct conduction pathway between the source and drain electrodes and the second is side-coupled to the first one by weak tunnel coupling, as illustrated in Fig. 1. This nanostructure, also known as the “side-coupled double quantum dot”, allows to study the interference between the direct and indirect conduction pathways (i.e., the Fano effect), as well as various correlation effects resulting from the strong electron-electron repulsion between the confined electrons, in particular the Kondo effect^{16–23}. Taking into account only the electron levels in close vicinity of the Fermi level, this system can be adequately described at low temperatures using a two-impurity Anderson model which is a simple extension of the single-impurity model that is commonly used for studying transport properties of single ultra-small quantum dots²⁴. The side-coupled double quantum dots have been intensively studied theoretically^{25–33}, uncovering a fascinating interplay between many-particle effects and quantum interference, however the first experimental study of this system has been performed only very recently (Ref. 34). Most previous

theoretical works consider the zero-bias conductance in the zero-temperature limit, while the experiment is decidedly performed at finite temperatures. It is known that this system is characterized by very low energy scales in some parameter regimes (in particular in the case of the two-stage Kondo effect^{27,28,35}), thus in order to properly describe its transport properties it is imperative to consider thermal effects and to calculate the conductance at finite temperatures using a non-perturbative method. This is the goal of the present work.

This paper is structured as follows. In Sec. II the model and the numerical renormalization group method are presented. The thermal effects are first studied in the non-interacting model in Sec. III, where we show that at finite temperatures the resonance line shape still has the Fano form to a good approximation, albeit with temperature-dependent parameters. In Sec. IV we then focus on the Fano-Kondo effect in the case where only the directly embedded quantum dot is interacting and experiences the Kondo screening; in this case the resonance line shape itself is appreciably modified by the combined Fano interference and Kondo effect. In Sec. V we finally study the fully interacting case, where completely different behavior is found. Finally, in Sec. VI the recent experimental results are examined and compared to theory, leading to the conclusion that the observed line-shape (an anti-resonance) is indicative of the occurrence of the two-stage Kondo effect.

II. MODEL AND METHOD

The Hamiltonian under study takes the following form:

$$\begin{aligned}
H = & \delta_d (n_d - 1) + \delta_a (n_a - 1) - t \sum_{\sigma} (d_{\sigma}^{\dagger} a_{\sigma} + \text{H.c.}) \\
& + \frac{U_d}{2} (n_d - 1)^2 + \frac{U_a}{2} (n_a - 1)^2 \\
& + \sum_{k\sigma} \epsilon_k c_{k\sigma}^{\dagger} c_{k\sigma} + V \sum_{k\sigma} (c_{k\sigma}^{\dagger} d_{\sigma} + \text{H.c.}),
\end{aligned} \quad (3)$$

where $n_d = \sum_{\sigma} d_{\sigma}^{\dagger} d_{\sigma}$ and $n_a = \sum_{\sigma} a_{\sigma}^{\dagger} a_{\sigma}$. The operators d_{σ}^{\dagger} and a_{σ}^{\dagger} are creation operators for an electron with spin σ on the embedded quantum dot d and on the side-coupled dot a , see Fig. 1. The on-site electron-electron repulsion is denoted by U_{α} , where α stands for d or a . The on-site energies ϵ_{α} of the dots are shifted by $U_{\alpha}/2$ in order to define the parameters

$$\delta_{\alpha} = \epsilon_{\alpha} + U_{\alpha}/2, \quad (4)$$

which measure the detuning from the particle-hole symmetric case which corresponds to $\delta_a = \delta_d = 0$. The coupling between the dots is described by the interdot tunnel coupling t . The dot d is assumed to couple to the source and drain electrodes in a symmetric way, thus it hybridizes with the even-parity combination of electrons from both leads^{16,36} with the strength

$$\Gamma_d = \pi \rho V^2, \quad (5)$$

which will be assumed to be constant for all energies within the conduction band of half-width D (equivalently, the den-

sity of states in the conduction band, ρ , is assumed to be constant, $\rho = 1/2D$). Throughout this work, Γ_d will be fixed to $\Gamma_d/D = 0.06$.

For the correct description of correlated regimes in clusters of quantum dots^{30,37-51,51-53} it is necessary to use non-perturbative techniques that take properly into account not only the local correlation effects on the impurity sites, but also the charge fluctuations and inter-site spin-spin coupling induced by the exchange interaction. One such technique is the numerical renormalization group (NRG)⁵⁴⁻⁶⁹ which involves three steps: 1) logarithmic discretization of the conduction band, 2) mapping onto a one-dimensional tight-binding chain with exponentially decreasing hopping constants, and 3) iterative diagonalization of the resulting Hamiltonian. The results presented in this work have been calculated using the NRG discretization parameter $\Lambda = 4$ with $N_z = 8$ equidistant values of the twist parameter z using an improved discretization scheme^{54,70}, with the truncation cutoff set at $10\omega_N$. The expectation values are calculated in the standard way, while the conductance curves at finite temperatures are computed using the Meir-Wingreen formula from the spectral data^{61,63,71}:

$$G(T) = G_0 \pi \Gamma_d \int_{-\infty}^{\infty} d\omega \left(-\frac{\partial f}{\partial \omega} \right) A_d(\omega, T), \quad (6)$$

where $G_0 = 2e^2/h$ is the conductance quantum (i.e., the conductance corresponding to full transmission), $f(\omega) = [1 + \exp(\beta\omega)]^{-1}$ is the Fermi function where $\beta = 1/k_B T$ and the chemical potential has been fixed at zero energy, and $A_d(\omega, T)$ is the spectral function on the impurity site d .

It should be noted that there is a significant conceptual difference as regards the usage of the Fano formula in the context of scattering experiments in atomic physics and the present context of nanoscopic transport. In atomic physics, the resonance is observed in the scattering cross-section as a function of the energy of the incoming particle while the resonance energy is fixed. In transport experiments, the resonance is observed in the conductance which relates to the scattering of electrons at the fixed energy of the Fermi level (this is strictly true only at zero temperature; at finite temperatures, electrons within an energy window of order $k_B T$ participate in the transport) and the independent variable is the energy of the side-coupled dot which is swept using gate voltages. In spite of the seemingly symmetric roles of parameters ϵ and ϵ_r in the expressions in Eqs. (1) and (2), there is a notable difference as regards the role of the background channel. The background scattering phase shift namely depends on the variable parameter in the first case, while it is essentially constant in the second case (at zero temperature). There may be some small variation of the background scattering phase shift when the parameters of the side-coupled dot are changed, since the two impurities are coupled and there will be hybridization effects induced by the side-coupled dot on the embedded dot. Nevertheless, this effect is rather small. We therefore conclude that any significant deviation from the universal Fano line-shape profile may only result from electron correlation effects or from thermal effects.

Furthermore, it should be remarked that the approach used in this work does not take into account that at high tempera-

tures the phase coherence necessary for the Fano interference may be partially lost, since full quantum coherence is assumed in solving the model^{13,72}. This implies that in experiments further reduction of the resonance amplitude is expected in addition to that found in our calculations which only take into account the effects due to the thermal broadening of the electron distribution function in the source and drain electrodes.

In the following, we set $k_B = 1$ and the conductance is always expressed in units of G_0 .

III. NON-INTERACTING CASE

The Fano formula has been originally formulated for a quantum system in its ground state. For a non-interacting system ($U_a = U_d = 0$), it is thus expected to describe the zero-temperature conductance essentially exactly as long as the background remains constant, which is the case if the Fano resonance is narrower than the Lorentzian spectral peak on the embedded quantum dot (of half-width Γ_d). The characteristic energy scale of the level broadening on the side-coupled quantum dot is

$$\gamma_a(\epsilon_a) = \pi A_d^0(\epsilon_a) t^2, \quad (7)$$

where $A_d^0(\omega)$ is the spectral function of the level d in the absence of the level a , which is given by

$$A_d^0(\omega) = \frac{1}{\pi \Gamma_d} \frac{1}{(\omega - \epsilon_d)^2 / \Gamma_d^2 + 1} \quad (8)$$

in the wide-band limit which applies well here for the chosen $\Gamma_d = 0.06D$. For later reference, we also give the full spectral function of the level d in the presence of the side-coupled dot:

$$A_d(\omega) = \frac{1}{\pi \Gamma_d} \frac{\Omega^2}{[1 - (\omega - \epsilon_d)(\omega - \epsilon_a)/t^2]^2 + \Omega^2}, \quad (9)$$

with $\Omega = (\omega - \epsilon_a)/(t^2/\Gamma_d)$.

The non-interacting case is also a good test for the NRG procedure, since a comparison with essentially exact results from simple quadrature of the spectral function is possible. We find that the results (detailed in the following subsections) are correct within the line-width or, more precisely, within less than half percent. A similar degree of precision is then also expected in the interacting case considered later on, since the NRG method functions equally well for any value of U .

A. Symmetric case, $\epsilon_d = 0$

Fixing $\epsilon_d = 0$ and taking the value of $A_d^0(\omega)$ at the Fermi level, $A_d^0(0) = 1/\pi\Gamma_d$, we obtain

$$\Gamma_a \equiv \gamma_a(0) = \frac{t^2}{\Gamma_d}. \quad (10)$$

The Fano formula applies for $\Gamma_a \ll \Gamma_d$, therefore the range of validity is expected to be given by $t \ll \Gamma_d$. In fact, for

$\epsilon_d = 0$ it turns out that the zero-temperature linear conductance $G(0) = G_0 \pi \Gamma_d A_d(0)$ reduces *exactly* to the Fano formula for any value of the t/Γ_d ratio:

$$G(0) = \frac{E^2}{1 + E^2}, \quad (11)$$

with $E = \epsilon_a/\Gamma_a$. The asymmetry parameter q is clearly zero, thus the Fano resonance takes the form of a symmetric anti-resonance.

The conductance curves for the non-interacting model with $\epsilon_d = 0$ are shown in Fig. 2a. At all temperatures, the resonance line-shape can be described with excellent accuracy using the Fano formula with temperature dependent parameters which are shown in Fig. 2b. The characteristic temperature scale for the temperature-dependence of the conductance curves is, as expected, Γ_a . An approximate expression for the temperature dependence of the resonance width in the temperature interval $[0 : \Gamma_a]$ is

$$\Gamma = \Gamma_a [1 + c_1(T/\Gamma_a)^2]^{c_2}, \quad (12)$$

with $c_1 = 9.2$ and $c_2 = 0.46$. This temperature-variation rule holds only in the $t/\Gamma_d \rightarrow 0$ limit: in general, the temperature variation also depends on the t/Γ_d ratio.

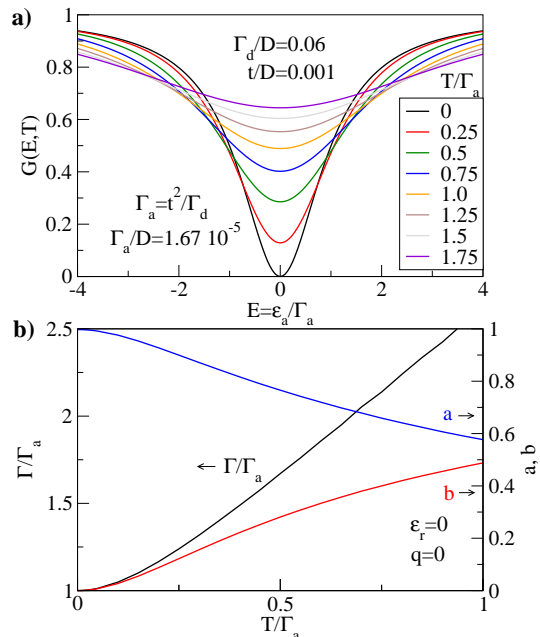


Figure 2: (Color online) Non-interacting model with $U_a = U_d = 0$, symmetric case, $\epsilon_d = 0$. a) Conductance curves for a range of temperatures. Fano-resonance-line fits overlap completely with the conductance curves. b) Fano parameters as a function of the temperature.

We have verified that for $\epsilon_d = 0$ the Fano curve accurately describes the finite-temperature conductance even for t of the order of Γ_d (results not shown).

B. Asymmetric case, $\epsilon_d \neq 0$

For $\epsilon_d \neq 0$, the d -level Lorentzian is no longer fixed at the Fermi level, which has a number of significant consequences. The effective level broadening on the side-coupled dot is reduced and it is given by

$$\Gamma_a \equiv \gamma_a(0) = \frac{t^2}{\Gamma_d} \frac{1}{(\epsilon_d/\Gamma_d)^2 + 1}. \quad (13)$$

Furthermore, the background phase shift is no longer $\pi/2$, thus the asymmetry parameter q is different from 0. From Eq. (9) it is clear that the zero-temperature conductance is always zero at $\epsilon_a = 0$, however the actual resonance energy ϵ_r is actually shifted away from zero. In fact, within an error of order t^2/Γ_d^2 , the following Fano parameters hold at $T = 0$ for general ϵ_d :

$$\begin{aligned} \epsilon_r &= \epsilon_d, \\ \Gamma &= \Gamma_a, \\ q &= \epsilon_d/\Gamma_d, \\ a &= \frac{1}{1 + (\epsilon_d/\Gamma_d)^2}, \\ b &= 0. \end{aligned} \quad (14)$$

The results of a temperature-dependent calculation for $\epsilon_d/\Gamma_d = 0.5$ are shown in Fig. 3. We observe a departure from the Fano line-shape which grows as the temperature is increased; nevertheless, the departure is small and it is still meaningful to perform curve fitting using the Fano formula. Similar to the symmetric $\epsilon_d = 0$ case, the main effect of finite temperature is to increase the width of the Fano resonance beyond Γ_a and to reduce the amplitude of the resonance. The asymmetry parameter q is, however, nearly constant: it reduces from $q = 0.5$ at zero temperature to $q = 0.47$ at $T = \Gamma_a$, while in the same temperature interval the amplitude is reduced by half. The resonance position, as given by ϵ_r , is also affected rather weakly. Such behavior is characteristic of the $t \ll \Gamma_d$ limit. For larger t , the extracted Fano parameters q and ϵ_r are more strongly temperature dependent, however the deviation from the Fano profile remains small (results not shown).

We conclude, fully in line with the expectations, that in the non-interacting case the main effect of finite temperature is to reduce the amplitude and increase the width of the resonance, while the Fano line-shape is largely preserved. As we show in the following, this is no longer the case in the presence of interactions, except in some special limits.

IV. INTERACTING CASE WITH $U_d \neq 0$ AND $U_a = 0$

The occurrence of the Fano resonance in transport problems is always associated with changes of the charge state of the weakly coupled discrete state. For this reason, there is a significant difference between the $U_a \ll \Gamma_a$ and $U_a \gg \Gamma_a$ situations. In the first limit, the occupancy changes by 2

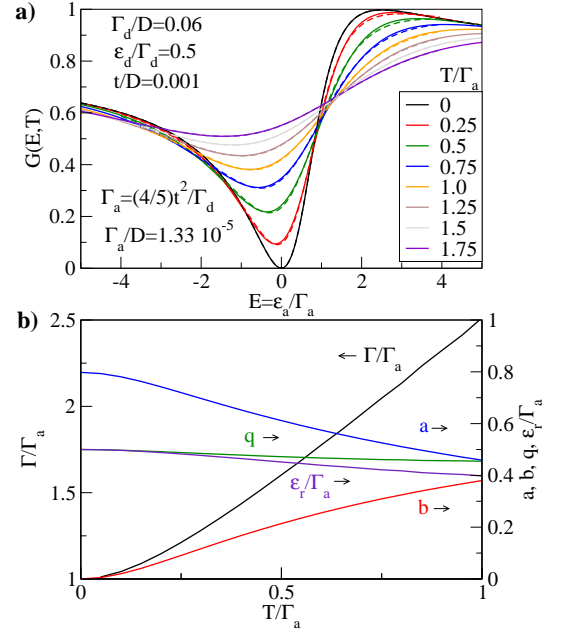


Figure 3: (Color online) Non-interacting model with $U_a = U_d = 0$, asymmetric case, $\epsilon_d \neq 0$. a) Conductance curves for a range of temperatures. Full curves: NRG results. Dashed lines: Fano resonance line fits. b) Fano parameters as a function of the temperature. Parameters are extracted by curve fitting in the energy window which corresponds to the horizontal axis in the upper subfigure.

(by one electron for each spin orientation) as ϵ_a crosses the Fermi level, thus the phase change in each spin channel is π : this corresponds to the usual Fano-resonance scenario. In the second limit, the total occupancy changes only by one due to the electron-electron repulsion preventing the second electron from entering the quantum dot. This corresponds to a $\pi/2$ phase shift in each spin channel and, roughly speaking, only one half of the Fano-resonance-like feature is expected to be seen. In this section we discuss the first case, i.e., the $U_a \ll \Gamma_a$ limit, which we study by setting U_a to zero.

When the embedded dot is tuned to its particle-hole symmetric point ($\delta_d = 0$), the impurity spectral function A_d^0 is pinned at the Fermi level to the value of $1/\pi\Gamma_d$ irrespective of the value of the electron-electron repulsion U_d . This is true even for moderate departures from the particle-hole symmetric point, $|\delta_d| \lesssim U_d/2$, since the Kondo resonance remains near the Fermi level, unlike the Lorentzian peak in the non-interacting case. For small t , the characteristic energy scale of the side-coupled quantum dot is therefore still $\Gamma_a = t^2/\Gamma_d$ as in the symmetric non-interacting case. For larger t the broadening will, however, eventually become comparable to the width of the Kondo resonance (of order T_K^0). The behavior therefore depends on the ratio between the hybridization of the side-coupled dot Γ_a and the Kondo temperature of the decoupled embedded dot, T_K^0 . If $\Gamma_a \ll T_K^0$, the physics of the embedded dot will not be affected much by the side-coupled dot (and vice versa), thus the conductance as a function of ϵ_a will differ only slightly from the non-interacting case. This is illustrated in Fig. 4, upper panel, where we compare conduc-

tance curves for $U_d = 0$ and $U_d/D = 1$ at $t/D = 0.0001$, where $\Gamma_a/T_K^0 = 1.7 \times 10^{-3}$ since the Kondo temperature (Wilson's definition) is $T_K^0 = 9.7 \times 10^{-5}D$. In this regime the Kondo effect on the embedded dot in no way affects the Fano interference process in the relevant range of energies and temperatures (i.e. several times Γ_a). Only for very large ϵ_a and very high temperature (of the order of T_K^0) will the differences become apparent, however this is outside the parameter regime of interest here.

When Γ_a is equal to a considerable fraction of T_K^0 , we start to see small quantitative departure from the Fano line shape already for ϵ_a and T of the order of Γ_a , see Fig. 4, middle panel. This is clearly a consequence of the competition between correlation and interference effects, combined with further thermal effects. As expected, the discrepancy grows with increasing ϵ_a and T .

Finally, for $\Gamma_a \gg T_K^0$, the embedded dot is strongly perturbed by the coupling to the side-dot and the differences become drastic: at finite T , the line-shape differs qualitatively from the Fano form and, in particular, we observe the emergence of non-uniform E -dependence with broad humps around $E \sim \Gamma_a$.

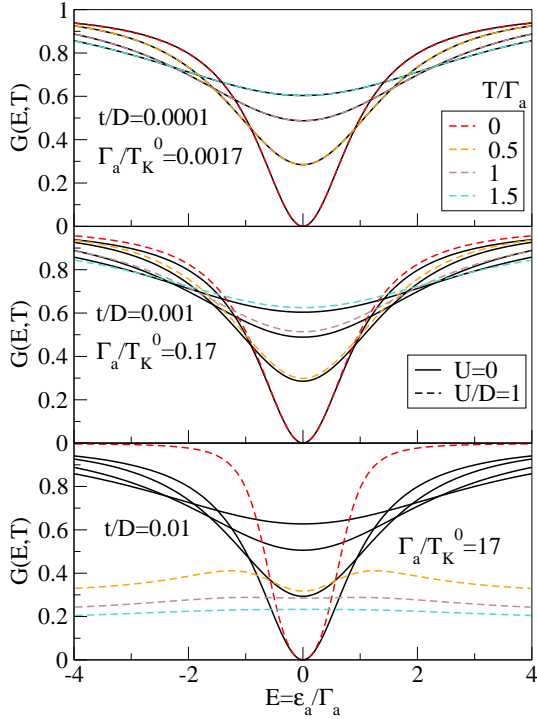


Figure 4: (Color online) Resonance curves for non-interacting (full lines) and interacting models (dashed lines) for a range of scaled temperatures T/Γ_a and for different Γ_a/T_K^0 ratios.

It is instructive to perform curve fitting on the results where the Fano resonance is already strongly perturbed, as shown in Fig. 5. The fits (shown using dashed lines), performed in the energy interval $[-4\Gamma_a : +4\Gamma_a]$, are clearly inadequate. Extracted Fano parameters indicate that the resonance width is significantly reduced below Γ_a and its width even decreases with increasing temperature, which reflects the sit-

uation where the spectral function of the embedded dot has a significant variation on the energy scale of Γ_a , which affects the resonance line-shape for large E . It should also be noted that parameters a and b have “unphysical” values $a > 1$ and $b < 0$ for small T . If the curve fitting is performed in a narrower energy interval $[-\Gamma_a : +\Gamma_a]$, the asymptotic small- E form of the resonance can be well captured, however the extracted Fano parameters are factitious and therefore of little use. This demonstrates that in the presence of strong competition between the Fano interference and Kondo effect, the curve fitting using the Fano line-shape is not recommended since the results depend very strongly on the energy window where fitting is performed and it is thus not advisable to make any inference based on them.

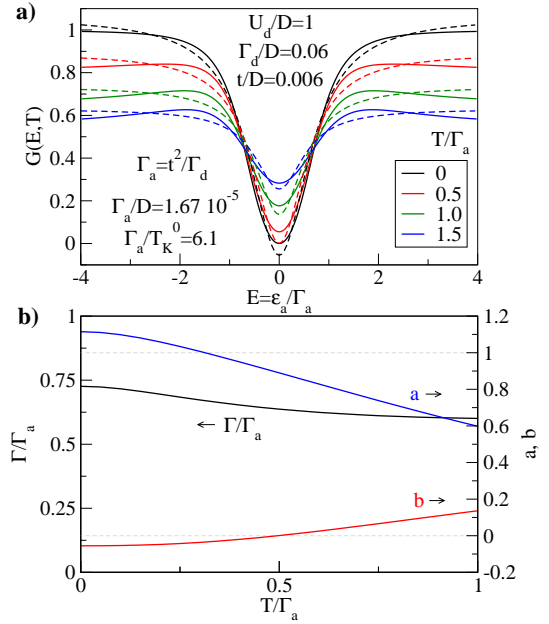


Figure 5: (Color online) Interacting model with $U_d \neq 0$ and $U_a = 0$. Symmetric case, $\epsilon_d = 0$. a) Conductance curves for a range of temperatures. b) Fano parameters as a function of the temperature. Curve fitting is performed in the energy window which corresponds to the horizontal axis in the upper subfigure.

Since there are two different energy scales in the problem (T_K^0 and Γ_a), the temperature-dependence of the conductance is expected to be non-monotonic, as shown in Fig. 6 where we plot the conductance at the bottom of the Fano anti-resonance (i.e. for $\epsilon_a = 0$). Such dependence is a consequence of the competition between the Kondo and Fano effects. The Kondo effect tends to increase the conductance through the formation of many-particle resonance at the Fermi level which opens a new conduction channel through the system. On the other hand, the Fano effect suppresses the conductance through quantum interference. For $T_K^0 \gg \Gamma_a$, the conductance first increases at the higher temperature scale of T_K^0 (the temperature dependence being given by the universal Kondo conductance curve⁷¹), then it decreases at the lower temperature scale set by Γ_a : see results for $t/D = 0.0001$ and $t/D = 0.001$ in Fig. 6. Note that the unitary limit of full conductance quantum

is not achieved at intermediate temperatures even in the case of well separated energy scales (three orders of magnitude for $t/D = 0.0001$). For larger t , the conductance peaks near $T \sim \Gamma_a$, where both competing effects are equally suppressed by thermal fluctuations.

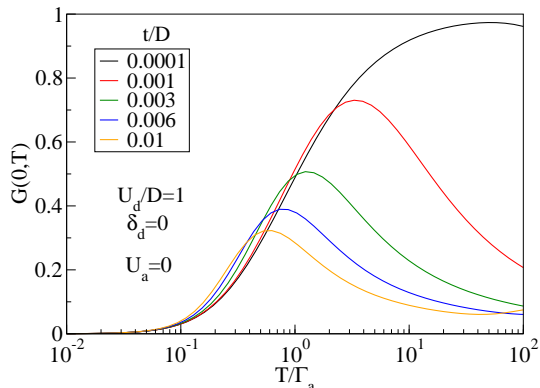


Figure 6: (Color online) Temperature-dependence of the conductance for $\epsilon_a = 0$, i.e. at the bottom of the conductance anti-resonance, for a range of the inter-dot coupling strengths.

It is also worthwhile to compare the temperature-dependence of the conductance $G(T)$ with the energy-dependence of the zero-temperature spectral function $A_d(\omega, T = 0)$, see Fig. 7. A common approximation in discussing the transport properties of quantum dot systems is to assume that the temperature variation of the conductance simply follows the energy variation of the zero-temperature spectral function, i.e., $G(T) \approx \pi\Gamma_d A_d(T, 0)$. While this is true on the qualitative level, the numerical results shown significant qualitative differences: the conductance curves are generally significantly broader and, accordingly, their maxima are lower. In particular, while the spectral function often attains values very close to $1/\pi\Gamma_d$ in some frequency range, the conductance is not unitary in the corresponding temperature range.

The parameter regime studied in this section corresponds to the model used in Ref. 34 to obtain the conductance plots featuring an anti-resonance, which were proposed to explain the experimentally observed Fano-resonance-like line shapes with small q . It can be noticed, however, that this parameter regime is not appropriate, since it corresponds to a change of occupancy of the side dot by 2, while from the experimentally observed honeycomb stability diagram one can deduce that the electron number changes only by one. We return to this issue in Sec. VI.

V. FULLY INTERACTING CASE

We first study the effect of finite electron-electron repulsion on the side-coupled dot in the case where the embedded dot itself is non-interacting, $U_d = 0$. In this way we exclude all processes related to the inter-dot exchange interaction and we may focus on the path-interference physics.

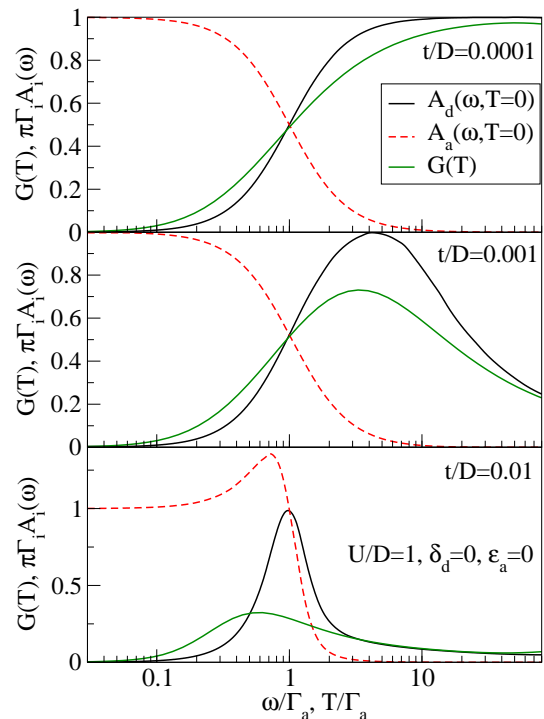


Figure 7: (Color online) Comparison of the temperature-dependence of the conductance $G(T)$ with the energy-dependence of the zero-temperature spectral function on the embedded dot $A_d(\omega, T = 0)$. For completeness, the spectral function on the side-coupled dot $A_a(\omega, T = 0)$ is also shown. Spectral functions are rescaled in units of the respective effective hybridisation strength, i.e., by $1/\pi\Gamma_i$, where $i \in \{a, d\}$. Conductance curves are rescaled in units of the conductance quantum $G_0 = 2e^2/h$. The horizontal axis is rescaled in units of $\Gamma_a = t^2/\Gamma_d$ (note that Γ_a is different in each subfigure).

To simplify the discussion, we focus solely on the symmetric case with $\epsilon_d = 0$. As previously discussed, as long as $U_a \ll \Gamma_a$, the side-coupled dot is essentially non-interacting and the results are equivalent to those shown in Sec. III A. For larger $U_a > \pi\Gamma_a$, however, the side-coupled dot will undergo the Kondo effect and its occupancy will be pinned to 1 for ϵ_a below several times Γ_a . Consequently, the “resonance” line-shape in this regime will take the form of an inverted “Kondo plateau onset”. The evolution from the Fano resonance to the Kondo plateau onset is shown in the upper left panel in Fig. 8, while the associated level occupancy curves are shown in the bottom left panel. (See also Fig. 3 in Ref. 53 where a similar setup is considered.)

We now finally discuss the fully interacting case, which is the situation which is relevant for the actual experimental configuration. The results are shown in the right panels in Fig. 8. We find a very similar evolution in the conductance and occupancy curves with increasing U_a as in the $U_d = 0$ case. The transition from the Fano line shape to the Kondo plateau-edge shape occurs in this case for lower values U_a , however, and already by $U_a/D = 0.01$ we obtain conductance curves which do not change much as U_a is further increased. This is very important since it implies that the regime of significantly large

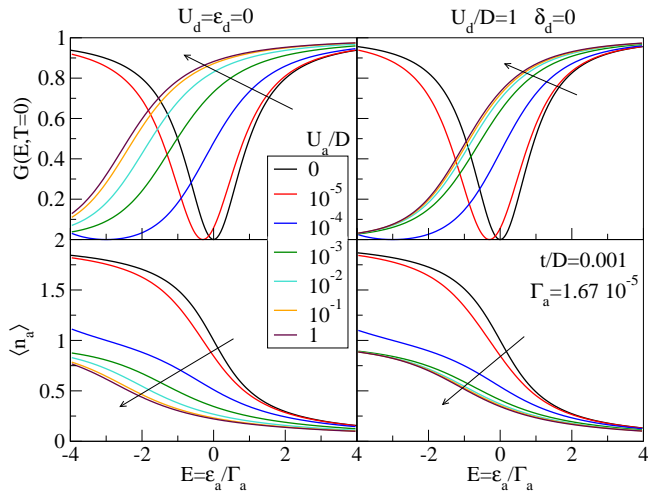


Figure 8: (Color online) Conductance curves and level-occupancies at $T = 0$ for a range of electron-electron interaction strengths U_a . Left panels: non-interacting embedded impurity. Right panels: interacting embedded impurity. The arrows show the direction of increasing U_a .

U_a occurs for rather small values of U_a , therefore it is not appropriate to model the side-coupled dot as a non-interacting impurity, since it is unlikely that the electron-electron repulsion in two similar quantum dots would differ by orders of the magnitude. We now face a dilemma: assuming a non-interacting side-coupled dot, we obtain conductance curves which appear to agree with the experimental results (albeit we know that they correspond to a change of occupancy by 2, in contradiction with the experimental situation), while assuming an interacting side-coupled dot, we obtain very different results which are in strong disagreement with those actually observed.

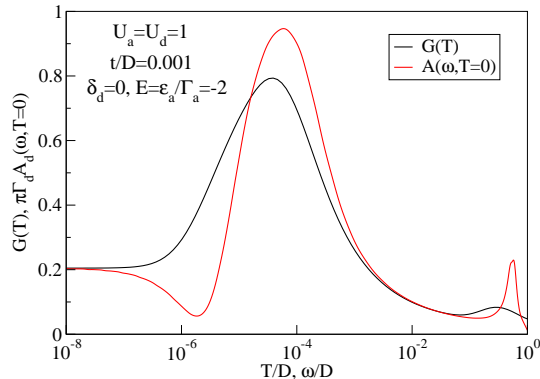


Figure 9: (Color online) Comparison of the temperature-dependence of the conductance $G(T)$ with the energy-dependence of the zero-temperature spectral function on the embedded dot $A_d(\omega, T = 0)$.

In Fig. 9 we compare the temperature dependence $G(T)$ with the energy-dependence of the $T = 0$ spectral function $A_d(\omega, T = 0)$. As before (cf. Fig. 7 and the related discussion), we observe that in spite of a certain general similarity between the curves, the differences are notable. In this

case, the differences are even qualitative: while $G(T)$ exhibits two ranges of logarithmic behavior (the first Kondo screening stage from $10^{-4} < T < 10^{-2}$, and the second Kondo screening stage from $10^{-6} < T < 10^{-4}$), the zero-temperature spectral function is more complex and even attains a minimum at $\omega \approx 2 \times 10^{-6}$ before increasing back to its asymptotic value at the Fermi level. This complex behavior is *not* reflected in the temperature dependence of the transport properties. Additional calculations (results not shown) indicate that $G(T)$ and $A_d(\omega, T = 0)$ are very similar only in vicinity of the particle-hole symmetric point, and even there only when the two Kondo temperature scales are well separated. This should serve as a caveat: since $G(T)$ is a convolution of the *finite-temperature* spectral function, see Eq. (6), it is not expected that, in general, all the details of the energy-dependence of the zero-temperature spectral function will manifest as similar variations in the temperature-dependence of the conductance at the related temperatures.

VI. RELATION TO THE EXPERIMENTAL RESULTS

Since the experiment is performed at finite temperatures, the results for the zero-temperature conductance can be very misleading in problems with very low energy scales⁵⁰. This commonly occurs in the side-coupling geometry and in clusters of quantum dot with weak inter-dot tunnel coupling^{27,28,48,50}. In Fig. 10a) we thus plot the conductance for a range of finite temperatures, which reveals completely different transport properties when compared with the zero-temperature limit.

When both quantum dots are interacting and the parameters are set in such a way that local moments form on both dots, there is a possibility that the Kondo screening will proceed in two steps^{26,28,29,48,50,52,73}: at higher Kondo temperature T_K^0 , the moment on the first dot will be screened, while another stage of Kondo screening of the moment on the side-coupled second dot occurs at another much lower energy scale $T_K^{2,28,73}$:

$$T_K^2 = c_1 T_K^0 \exp(-c_2 T_K^0 / J_{\text{eff}}), \quad (15)$$

where c_1 and c_2 are some constants of the order 1. Such *two-stage Kondo screening* occurs if the effective Kondo exchange coupling J_{eff} of the spin on the second dot with the quasiparticles resulting from the first stage is lower than T_K^0 . In this case, the second Kondo scale may be pushed to exponentially low temperature T_K^2 . The exchange coupling

$$J_{\text{eff}} = \frac{2t^2}{\epsilon_a - \epsilon_d + U_a} + \frac{2t^2}{\epsilon_d - \epsilon_a + U_d} \quad (16)$$

depends on the value of ϵ_a and decreases as ϵ_a is reduced, attaining its minimum for $\epsilon_a = \delta_d - U_a/2$. In turn, this implies that T_K^2 becomes very low for small ϵ_a , thus at the experimentally relevant temperatures the second stage of Kondo screening does not occur, the conductance suppression does not arise and the conductance curve takes a form similar to that of the Fano resonance. In experiments, the temperature is roughly one order of the magnitude lower than the Kondo

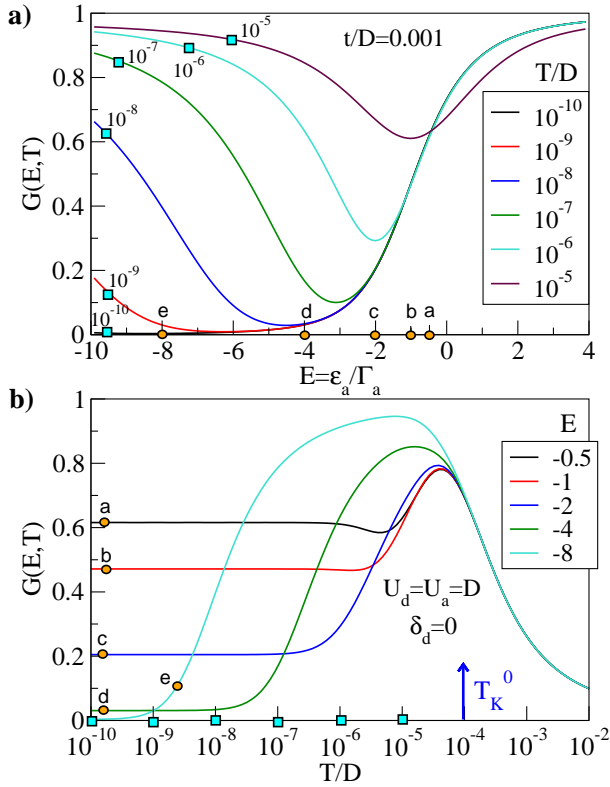


Figure 10: (Color online) a) Conductance curves for the fully interacting case with $U_d/D = U_a/D = 1$, $\delta_d = 0$, for a range of different temperatures. b) Temperature dependence of the conductance for a range of energies of the side-coupled dot.

temperature; for chosen $t/D = 0.001$, we indeed find that for $T/D = 10^{-5} \approx 0.1T_K^0$, the conductance form takes the form of a nearly symmetric anti-resonance, in agreement with the experiment. The minimum of the anti-resonance is located at lower value of $E = \epsilon_a/\Gamma_a$ as compared to the non-interacting case (where it is found exactly at $E = 0$), since the physical mechanism for its occurrence is completely different: in the non-interacting case we observe a *complete* suppression of the conductance due to quantum interference between different conductance pathways, while in the interacting case the *incomplete* suppression results from the separation of the energy scales T_K^0 and T_K^2 with the experimental temperature set on an intermediate scale so that $T_K^2 < T < T_K^0$. The shift from $E = 0$ is not observable experimentally, since the exact value of the parameter ϵ_a is not known: it has to be inferred indirectly from known gate voltages on the electrodes and the capacitances.

If the inter-dot tunneling t is increased so that the exchange coupling becomes comparable or exceeds the Kondo temperature, the conductance curves no longer exhibit a Fano-like anti-resonance, not even at elevated temperatures, see Fig. 11. Instead, as E is reduced so that the side-coupled dot becomes occupied by one electron, the two electrons (one from each quantum dot) bind to a local singlet on the temperature scale of $J \sim 4t^2/U$ and there are no other lower temperature scales.

The interpretation of the anti-resonance in terms of a ther-

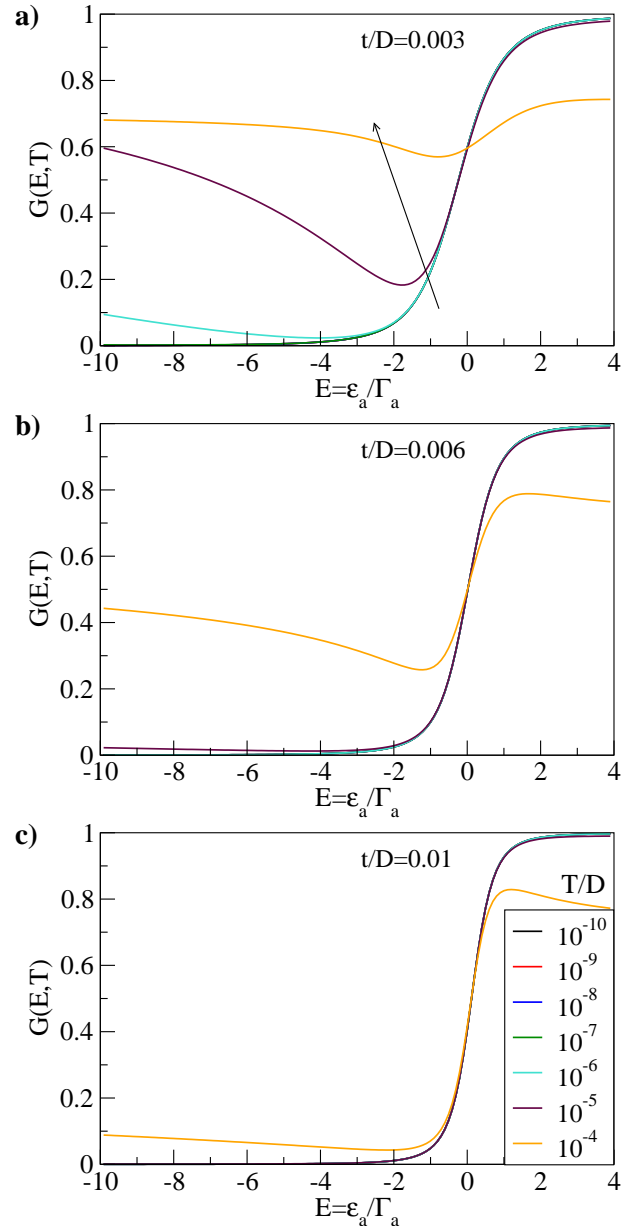


Figure 11: (Color online) Conductance curves for the fully interacting case with $U_d/D = U_a/D = 1$, $\delta_d = 0$, for increasing inter-dot tunneling t . The arrow indicates the direction of the increasing temperature T .

mally suppressed second-stage Kondo screening is supported by the experimental results for the temperature-dependence of the resonant conductance (Fig. 2c in Ref. 34) which indicate a logarithmic behavior. This temperature variation corresponds to the high-temperature range in Fig. 10b). The experimental results do not indicate any saturation of G for the lowest experimentally accessible temperatures, however this might simply indicate that the temperature is not sufficiently below T_K , or that t is indeed very small and thus T_K^2 is exponentially low. Further confirmation for the interpretation in terms of the two-stage Kondo effect could be obtained by also consid-

ering the temperature-dependence of other parameters which determine the anti-resonance line-shape; the variations of amplitude, width, and asymmetry parameter should all exhibit logarithmic temperature dependence.

In addition to the thermal effects, the second stage of Kondo screening may also be suppressed by a minute magnetic field such that $T_K^2 \ll B \ll T_K^0$. As it is likely that there are always some small stray magnetic fields in the experimental device, this provides another mechanism which tends to produce Fano-resonance-like spectral features in the present configuration.

VII. CONCLUSION

The transport properties of a system of two quantum dots in the side-coupled geometry have been analyzed, focusing on the parameter range where the occupancy of the side-coupled dot changes as its energy crosses the Fermi level. The re-

sulting resonance line-shapes in the conductance curves have been comprehensively studied in various parameter regimes for both non-interacting and interacting quantum dots. We find an alternative interpretation of the experimental results from Ref. 34 which fulfils the two required conditions: 1) the occupancy in the side-coupled dot changes by one, 2) the resonance line-shape features a weakly asymmetric Fano-like anti-resonance. The proposed model takes into account the electron-electron interaction on the side-coupled dot, which is certainly present in the experimental device and which has been shown in this work to be relevant for the transport properties of the system.

Acknowledgments

The author acknowledges the support of the Slovenian Research Agency (ARRS) under Grant No. Z1-2058.

-
- ¹ U. Fano, Phys. Rev. **124**, 1866 (1961).
² A. E. Miroschnichenko, S. Flach, and Y. S. Kivshar, *Fano resonance in nanoscale structures*, arxiv:0902.3014 (2009).
³ K. Kang, S. Y. Cho, J.-J. Kim, and S.-C. Shin, Phys. Rev. B **63**, 113304 (2001).
⁴ M. E. Torio, K. Hallberg, S. Flach, A. E. Miroschnichenko, and M. Titov, Eur. Phys. J. B **37**, 399 (2004).
⁵ A. A. Aligia and L. A. Salguero, Phys. Rev. B **70**, 075307 (2004).
⁶ A. C. Johnson, C. M. Marcus, M. P. Hanson, and A. C. Gossard, Phys. Rev. Lett. **93**, 106803 (2004).
⁷ M. Sato, H. Aikawa, K. Kobayashi, S. Katsumoto, and Y. Iye, Phys. Rev. Lett. **95**, 066801 (2005).
⁸ P. A. Orellana, G. A. Lara, and E. V. Anda, Phys. Rev. B **74**, 193315 (2006).
⁹ K. Kobayashi, H. Aikawa, S. Katsumoto, and Y. Iye, Phys. Rev. Lett. **88**, 256806 (2002).
¹⁰ B. R. Bulka and P. Stefanski, Phys. Rev. Lett. **86**, 5128 (2001).
¹¹ A. A. Aligia and C. R. Proetto, Phys. Rev. B **65**, 165305 (2002).
¹² M. E. Torio, K. Hallberg, A. H. Ceccatto, and C. R. Proetto, Phys. Rev. B **65**, 085302 (2002).
¹³ K. Kobayashi, H. Aikawa, A. Sano, S. Katsumoto, and Y. Iye, Phys. Rev. B **70**, 035319 (2004).
¹⁴ I. Maruyama, N. Shibata, and K. Ueda, J. Phys. Soc. Jpn. **73**, 3239 (2004).
¹⁵ T. Lobo, M. S. Figueira, and M. E. Foglio, Nanotechnology **17**, 6016 (2006).
¹⁶ L. I. Glazman and M. E. Raikh, JETP Lett. **47**, 452 (1988).
¹⁷ S. M. Cronenwett, T. H. Oosterkamp, and L. P. Kouwenhoven, Science **281**, 540 (1998).
¹⁸ D. Goldhaber-Gordon, H. Shtrikman, D. Mahalu, D. Abusch-Magder, U. Meirav, and M. A. Kastner, Nature **391**, 156 (1998).
¹⁹ D. Goldhaber-Gordon, J. Göres, M. A. Kastner, H. Shtrikman, D. Mahalu, and U. Meirav, Phys. Rev. Lett. **81**, 5225 (1998).
²⁰ W. G. van der Wiel, S. D. Franceschi, T. Fujisawa, J. M. Elzerman, S. Tarucha, and L. P. Kouwenhoven, Science **289**, 2105 (2000).
²¹ H. Jeong, A. M. Chang, and M. R. Melloch, Science **293**, 2221 (2001).
²² L. Kouwenhoven and L. Glazman, Physics World **Jan**, 33 (2001).
²³ A. C. Hewson, *The Kondo Problem to Heavy-Fermions* (Cambridge University Press, Cambridge, 1993).
²⁴ W. G. van der Wiel, S. D. Franceschi, J. M. Elzerman, T. Fujisawa, S. Tarucha, and L. P. Kouwenhoven, Rev. Mod. Phys. **75**, 1 (2003).
²⁵ D. Boese, W. Hofstetter, and H. Schoeller, Phys. Rev. B **66**, 125315 (2002).
²⁶ M. Vojta, R. Bulla, and W. Hofstetter, Phys. Rev. B **65**, 140405(R) (2002).
²⁷ P. S. Cornaglia and D. R. Grempel, Phys. Rev. B **71**, 075305 (2005).
²⁸ R. Žitko and J. Bonča, Phys. Rev. B **73**, 035332 (2006).
²⁹ R. Žitko and J. Bonča, J. Phys.: Condens. Matter **19**, 255205 (2007).
³⁰ C. Karrasch, T. Enss, and V. Meden, Phys. Rev. B **73**, 235337 (2006).
³¹ P. Stefanski, A. Tagliacozzo, and B. R. Bulka, Phys. Rev. Lett. **93**, 186805 (2004).
³² Y. Tanaka and N. Kawakami, Phys. Rev. B **72**, 085304 (2005).
³³ M. Weyrauch and D. Sibold, Phys. Rev. B **77**, 125309 (2008).
³⁴ S. Sasaki, H. Tamura, T. Akazaki, and T. Fujisawa, Phys. Rev. Lett. **103**, 266806 (2009).
³⁵ C.-H. Chung, G. Zaránd, and P. Wölfle, Phys. Rev. B **77**, 035120 (2008).
³⁶ M. Pustilnik and L. Glazman, J. Phys.: Condens. Matter **16**, R513 (2004).
³⁷ W. Izumida and O. Sakai, Phys. Rev. B **62**, 10260 (2000).
³⁸ L. Borda, G. Zaránd, W. Hofstetter, B. I. Halperin, and J. von Delft, Phys. Rev. Lett. **90**, 026602 (2003).
³⁹ M. R. Galpin, D. E. Logan, and H. R. Krishnamurthy, Phys. Rev. Lett. **94**, 186406 (2005).
⁴⁰ A. Oguri and A. C. Hewson, J. Phys. Soc. Japan **74**, 988 (2005).
⁴¹ J. Mravlje, A. Ramšak, and T. Rejec, Phys. Rev. B **73**, 241305(R) (2006).
⁴² R. Žitko, J. Bonča, A. Ramšak, and T. Rejec, Phys. Rev. B **73**, 153307 (2006).
⁴³ Y. Nisikawa and A. Oguri, Phys. Rev. B **73**, 125108 (2006).
⁴⁴ G. Zaránd, C.-H. Chung, P. Simon, and M. Vojta, Phys. Rev. Lett. **97**, 166802 (2006).
⁴⁵ R. Žitko and J. Bonča, Phys. Rev. B **74**, 045312 (2006).
⁴⁶ L. G. G. V. Dias da Silva, N. P. Sandler, K. Ingersent, and S. E.

- Ulloa, Phys. Rev. Lett. **97**, 096603 (2006).
- ⁴⁷ R. Žitko and J. Bonča, Phys. Rev. B **76**, 241305(R) (2007).
- ⁴⁸ R. Žitko and J. Bonča, Phys. Rev. Lett. **98**, 047203 (2007).
- ⁴⁹ A. M. Lobos and A. A. Aligia, Phys. Rev. B **74**, 165417 (2006).
- ⁵⁰ R. Žitko and J. Bonča, Phys. Rev. B **77**, 245112 (2008).
- ⁵¹ G. B. Martins, C. A. Büsser, K. A. Al-Hassanieh, E. V. Anda, A. Moreo, and E. Dagotto, Phys. Rev. Lett. **96**, 066802 (2006).
- ⁵² E. V. Anda, G. Chiappe, C. A. Büsser, M. A. Davidovich, G. B. Martins, F. Heidrich-Meisner, and E. Dagotto, Phys. Rev. B **78**, 085308 (2008).
- ⁵³ L. G. G. V. Dias da Silva, K. Ingersent, N. Sandler, and S. E. Ulloa, Phys. Rev. B **78**, 153304 (2008).
- ⁵⁴ R. Žitko and T. Pruschke, Phys. Rev. B **79**, 085106 (2009).
- ⁵⁵ K. G. Wilson, Rev. Mod. Phys. **47**, 773 (1975).
- ⁵⁶ H. R. Krishna-murthy, J. W. Wilkins, and K. G. Wilson, Phys. Rev. Lett. **35**, 1101 (1975).
- ⁵⁷ H. R. Krishna-murthy, J. W. Wilkins, and K. G. Wilson, Phys. Rev. B **21**, 1003 (1980).
- ⁵⁸ H. R. Krishna-murthy, J. W. Wilkins, and K. G. Wilson, Phys. Rev. B **21**, 1044 (1980).
- ⁵⁹ M. Yoshida, M. A. Whitaker, and L. N. Oliveira, Phys. Rev. B **41**, 9403 (1990).
- ⁶⁰ W. C. Oliveira and L. N. Oliveira, Phys. Rev. B **49**, 11986 (1994).
- ⁶¹ T. A. Costi, A. C. Hewson, and V. Zlatic, J. Phys.: Condens. Matter **6**, 2519 (1994).
- ⁶² R. Bulla, A. C. Hewson, and T. Pruschke, J. Phys.: Condens. Matter **10**, 8365 (1998).
- ⁶³ T. A. Costi, Phys. Rev. B **64**, 241310(R) (2001).
- ⁶⁴ W. Hofstetter, Phys. Rev. Lett. **85**, 1508 (2000).
- ⁶⁵ W. Izumida and O. Sakai, J. Phys. Soc. Japan **74**, 103 (2005).
- ⁶⁶ R. Peters, T. Pruschke, and F. B. Anders, Phys. Rev. B **74**, 245114 (2006).
- ⁶⁷ A. Weichselbaum and J. von Delft, Phys. Rev. Lett. **99**, 076402 (2007).
- ⁶⁸ R. Bulla, T. Costi, and T. Pruschke, Rev. Mod. Phys. **80**, 395 (2008).
- ⁶⁹ V. L. Campo and L. N. Oliveira, Phys. Rev. B **72**, 104432 (2005).
- ⁷⁰ R. Žitko, Comp. Phys. Comm. **180**, 1271 (2009).
- ⁷¹ M. Yoshida, A. C. Seridonio, and L. N. Oliveira, Phys. Rev. B **80**, 235317 (2009).
- ⁷² I. G. Zacharia, D. Goldhaber-Gordon, G. Granger, M. A. Kastner, Y. B. Khavin, H. Shtrikman, D. Mahalu, and U. Meirav, Phys. Rev. B **64**, 155311 (2001).
- ⁷³ P. S. Cornaglia, D. R. Grempel, and H. Ness, Phys. Rev. B **71**, 075320 (2005).
- ⁷⁴ In line with the convention followed by the quantum impurity physics community, the hybridization strength Γ is defined in this work as the resonance half-width. This needs to be contrasted with the convention where Γ is taken to be the full-width (i.e., level broadening) which is more commonly used by experimentalists. In the letter case, one has $E = (\epsilon - \epsilon_r)/(\Gamma/2)$.